

Potassium and zeolitic structure modified ultra-microporous adsorbent materials from a renewable feedstock with favourable surface chemistry for CO₂ capture

Xin Liu^a, Yuan Sun^a, Jingjing Liu^a, Chenggong Sun^{a*}, Hao Liu^a, Qian Xue^a, Emily Smith^b, Colin Snape^a

a Faculty of Engineering, University of Nottingham, Nottingham NG7 2TU, UK

b School of Chemistry, Faculty of Science, University of Nottingham, Nottingham NG7 2RD, UK

Abstract: Novel hierarchically structured microporous bio-carbons with exceptionally high capacities for CO₂ capture have been synthesized from the abundant agricultural waste of rice husk (RH), using a facile methodology that effectively integrated carbonisation, activation and potassium intercalation into a one-step process. Textural characterisation demonstrates that the synthesized bio-carbons exhibit exceedingly high ultra-microporosity accounting for up to 95% of total porosity mainly as a result of the naturally occurring silicon compounds within the RH molecular framework structures. With a modest surface area of up to 1035 m²/g and a total pore volume of 0.43 cm³/g, the best performing RH carbon has showed exceptionally high and fully reversible CO₂ uptake capacity of 2.0 mmol/g at 25 °C and a CO₂ partial pressure of 0.15 bar, which represents one of the highest uptakes ever reported for both carbon and MOF materials usually prepared from using cost-prohibitive precursor materials with cumbersome methodologies. It has been found that up to 50% of the total CO₂ uptake is attributable to the unique surface chemistry of the RH carbons, which appears to be dominated by the enhanced formation of extra-framework potassium cations owing to the exceedingly high levels of ultra-microporosity and the presence of zeolitic structures incorporated within the carbon matrices. Characterisations by EDX element mapping, XPS and the heat of adsorption measurements confirm the existence of a range of zeolitic structures, which essentially transforms the RH carbons into a kind of zeolite-carbon nanocomposite materials with strong surface affinity to CO₂.

Keywords: CO₂ capture, carbon materials, rice husk, surface chemistry, ultra-microporosity

1 Introduction

The world faces unprecedented challenges in cutting the emissions of CO₂, the dominant greenhouse gas in the atmosphere from fossil fuel utilisation, which has clearly been taken as one of the major climate

change mitigation strategies. According to IEA and other climate change studies¹⁻³, in order to limit the rise in global temperature to 2 °C above pre-industrial levels, the global greenhouse gas emissions need to be reduced by 40 ~ 70% relative to 2010 by 2050, and to near-zero by 2100. Given the projected growing energy demand and continuous dominance of fossil fuels in foreseeable futures, it has generally been recognised that in addition to accelerating the application of renewable energy technologies and energy efficiency measures, carbon capture and storage (CCS) is the only viable option for decarbonising global power generation and other carbon-intensive process industries without compromising energy security while achieving climate change target^{1,4}. However, a number of technical and economic barriers will have to be overcome before CCS can be widely deployed on large scales. One of the major barriers is clearly the immaturity of affordable efficient technologies for carbon capture, which is the first and also the costliest element of the whole CCS chain. Among many CO₂ capture technologies currently under development at varying scales, adsorption-based post-combustion capture with solid adsorbents have been considered as a viable alternative to the state-of-art aqueous amine scrubbing, offering great promise for greatly improved process efficiency at reduced energy penalty and lower capital and operational cost. In addition, unlike toxic and corrosive amine solvents, the spent solid adsorbents can be effectively recycled or disposed of without undue environmental problems⁵.

For solid adsorbents-based capture systems either with pressure and/or temperature swing cycles, developing high-performance adsorbent materials has clearly become the focus of research, with the materials being investigated typically including activated carbons, zeolites, metal oxides, amine-based solid adsorbents, metal organic frameworks (MOFs) or polymers (MOPs) as well as zeolitic imidazolate frameworks (ZIFs)⁶⁻⁹. Among these adsorbent materials, carbon-based materials represent one of the most promising categories of adsorbents for CO₂ capture¹⁰⁻¹³, due to their large surface areas and pore volumes, high surface amenability, fast adsorption kinetics, low adsorption heat and hence ease of regeneration, high thermal and chemical stabilities, low moisture sensitivity and superior electrical and heat conductivities as well as the suitability for use in both pressure and temperature swing cycles. The adsorption performance of carbon-based materials is strongly affected both by their textural properties and surface chemistries, which are determined by many factors, such as the precursor materials, activation methodologies and post-preparation treatments^{8, 15, 16}. In general, as physical adsorbents,

activated carbons are usually very sensitive to flue gas temperatures and CO₂ partial pressures, with CO₂ adsorption capacities of most commercial carbons being usually below 5 wt% (ca. 1mmol/g) at 0.15 bar CO₂ and 25 °C despite their very high surface areas and pore volumes¹⁷⁻¹⁹. Therefore, increasing the surface affinities of carbon-based materials for CO₂ as a means to increase their adsorption capacities at low CO₂ partial pressures has become the focus of many investigations. One of the most popular methods is to use nitrogen-rich precursor materials to produce functional porous carbons, such as poly (benzoxazine-co-resol), polypyrrole, resorcinol–urea–formaldehyde resin, polybenzoxazine.¹⁹⁻²² The CO₂ adsorption capacities of the nitrogen-enriched carbon materials prepared with nitrogen contents being up to 22.3wt%, can have improved CO₂ uptake capacities varying between 1.3 and 1.8mmol/g at 25 °C and 0.15 bar CO₂, thanks to the formation of basic surface nitrogen functionalities, such as pyrrolic, pyridonic-N, pyridinic and quaternary nitrogen groups²¹⁻²⁴. MOFs and ZIFs were also used by some investigators to produce carbon-based CO₂ adsorbents by carbonisation at high temperatures but the CO₂ uptakes of the “designer” carbons at low CO₂ partial pressures showed no appreciable improvements, being typically only around 1.4mmol/g²⁵.

Various post-preparation treatments have also been investigated as a potential means to enhance surface affinity for CO₂, such as metal oxides doping and secondary activation with ammonia²⁶⁻²⁸, but only incremental improvements in CO₂ adsorption performance have been obtained, with CO₂ uptake being usually no more than 1.3mmol/g at low partial pressures. In our previous research¹⁶, we have reported that potassium intercalation, which can easily be achieved via an innovative chemical activation protocol, can be used as a facile but more powerful technique to greatly enhance the surface CO₂ affinity of carbon materials, leading to more than doubled CO₂ uptakes for nitrogen-free phenolic resin derived carbons. The results suggested that the greatly enhanced surface affinity for CO₂ is closely linked to the solid state electrostatic effects created by the extra framework cations due to alkali intercalation, a phenomenon that is usually only observed for zeolite and MOF adsorbent materials^{29,30}. Compared to other aforementioned carbon preparation and/or surface modification methodologies, alkali intercalation can potentially serve as a versatile and more effective approach for remarkably enhancing CO₂ capture performance of carbon-based adsorbents that can be produced from a wider range of feedstocks, such as various agricultural waste residues and other low-cost biomass and lignocellulosic wastes.

Biomass and other low cost agricultural wastes have increasingly become a preferred feedstock for activated carbon production but most bio-carbons are produced from using woody biomass³¹⁻³³. In this research, the use of alkali intercalation via chemical activation has been further developed as a novel methodology to produce alkali-intercalated functional carbon materials for CO₂ capture using the abundantly available low-cost agricultural waste of rice husk, which is produced at a scale of 140 million tonnes a year worldwide³⁴. Owing to its very low energy density on a volumetric dry basis³⁵, RH is usually considered as waste that is often dumped on landfills or destroyed in agricultural burning, although rice husk has been considered as a valuable resource for silica production due to its high silica content³⁶. In recent years, there have been some investigations into the use of rice husk to produce activated carbon materials for variable general applications, and chemical activation typically with alkali hydroxides or carbonates as being the activating agents has almost exclusively been used typically following a three-step process, namely carbonisation and activation followed by the removal of minerals by leaching³⁷⁻⁴⁰. However, to the best of our knowledge, no investigation has ever been carried out to use rice husk to prepare alkali-intercalated ultra-microporous materials for CO₂ adsorption by making the effective use of rice husk contained silicon as a natural template for deriving ultra-microporosity and by controlling the chemical activation to achieve alkali intercalation for further enhanced CO₂ uptake. In addition, in this research, the separate carbonisation and activation processes were effectively integrated into a single process to achieve simultaneous carbonisation and activation. It is our belief that alkali intercalation and ultra-microporosity can be better developed synergistically during the formation of carbon networks when these two separate processes are integrated.

2 Experimental

2.1 Preparation of activated carbon samples from rice husk

A batch of raw RH was sourced from China and used for the preparation of activated carbon samples. The raw RH sample was first dried, crashed and sieved into the particles in the range of 1.0-0.5mm. On a weight percentage basis, the RH sample has an ash content of 11.54% and contains 40.4% carbon, 5.70% hydrogen, 0.64% nitrogen, and 41.72% oxygen. The activating agents used, including technical grade potassium hydroxide (KOH) and potassium carbonate (K₂CO₃) were purchased from Sigma Aldrich.

An innovative chemical activation protocol, which can effectively facilitate the potassium intercalation during the activation process, was used to prepare the RH activated carbon samples. 3g of as-prepared raw RH sample was first physically mixed with activating agents at different mass ratios. The mixture was then heated up in a purpose-designed carbonisation/activation furnace to different pre-set final temperatures at a heating rate of 5 °C/min in a nitrogen flow of 1 L/min. Once the target temperature was reached, the sample mixture was maintained at this temperature for 1h before it was cooled down in N₂ to ambient conditions. To yield the final bio-carbon products, the mixture was removed from the activation furnace and washed till neutral with excessive quantities of de-ionized water (typically three times with 200 mL water). It was found that at the KOH/RH ratio of 1.0, the carbon yield ranged from 25% wt% at 600 °C, 20 wt% at 700 °C to 15 wt% at 800 °C. For activation with K₂CO₃, the yield is slightly higher by an average of 2 wt% than for KOH activation under the same conditions.

For the convenience of subsequent discussion, the carbons obtained from KOH and K₂CO₃ activation under different conditions are labelled as HC-X-Y and KC-X-Y respectively, where X represents the activation temperature and Y stands for the KOH/RH or K₂CO₃/RH mass ratios.

2.2 Characterisation

The textural properties of the prepared carbon samples were characterised with a Micromeritics ASAP 2420 instrument by N₂ and CO₂ adsorption at 77 and 273 K, respectively. Prior to the measurements, samples were first degassed at 120 °C for 16 hrs. The surface area was calculated by BET (Brunauer-Emmett-Teller) method using the N₂ adsorption isotherm data within the relative pressure ranging from 0.01 to 0.1. The cumulative pore volumes (V_{total}) were calculated from the amount of nitrogen adsorbed at P/P₀ of ca. 0.99. Since N₂ has diffusion problem at 77K to access narrow micropores, CO₂ adsorption isotherms at 0 °C was also applied to calculate narrow micropore volume and pore size distribution (PSD) using non-local density functional theory (NLDFT) model by a combination analysis of N₂ adsorption isotherms and CO₂ adsorption isotherms.

A JEOL 7100F FEG-SEM was employed to study the morphology of samples while high resolution transmission electron microscopy images were taken on JEOL 2100F FEG-TEM at 200 kV. Bruker S8 Tiger X-ray Fluorescence Spectrometer (XRF) was used for mineral elemental analysis for selected

samples. The structural and crystallographic properties of the RH carbons prepared in different conditions were examined with X-ray Diffraction (XRD) analysis (Bruker D8 Advance). The X-ray photoelectron spectroscopy measurements were performed using a Kratos AXIS Ultra DLD instrument. Samples were mounted on the standard Kratos sample bar using double sided tape (sellotape brand), these were inserted into the airlock and pumped down to $\sim 3 \times 10^{-7}$ Torr overnight before transfer into the instrument analysis chamber. The analysis chamber pressure during the measurements was better than 5×10^{-9} Torr.

2.3 CO₂ adsorption

A thermogravimetric analyser (Q500, TA instruments) was used to examine the CO₂ adsorption characteristics of the derived carbon samples. For each adsorption test, the sample was first dried at 120 °C in N₂ for 30 min before it was cooled down to 25 °C for CO₂ adsorption with the gas flow switched from N₂ to the simulated flue gas (15% CO₂ in N₂) at the same flow rate of 100 ml/min. Once the adsorption reached equilibrium at a given temperature, the sample was then heated up to 120 °C and held at this temperature till complete desorption. Cyclic adsorption and desorption tests were also conducted to study the stability and regenerability of the samples. In addition, CO₂ adsorption isotherms at 0 °C and 25 °C for different relative pressures was also measured using volumetric analysis (Micromeritics ASAP 2420) to characterise the surface CO₂ affinity of the carbon samples. ATG-DSC instrument (Setaram SENSYS evo) was used to measure the adsorption heat.

3 Results and Discussion

3.1 XRD and XRF characterisation

Fig. 1 shows the XRD pattern of the microcrystalline structure for the activated RH carbon samples obtained with different activation conditions. The broad and diffused peaks of the XRD profile demonstrate the disordered, amorphous structures of the carbons. Two broad characteristic peaks were observed, one centred at around 25° which corresponds to the (002) set of planes usually used to assess the pseudo graphic interlayer spacing and another at around 43°, corresponding to the microcrystalline lateral dimensions of (100) planes, respectively⁴¹⁻⁴⁴. It seems that at the activation temperature of 600 °C, increasing the KOH/RH mass ratio from 0.1 to 2 inflicted insignificant structural alterations in general,

despite the minor broadening observed for the (002) peak and the slightly increased 100 peak corresponding to the lateral dimension of graphitic crystallites. However, the effect of the activation temperature was found to be significantly greater. It was found that when the activation temperature increased from 600 to 800°C at a given KOH/RH mass ratio, the (002) peak became increasingly broader and weaker or even disappeared whilst the (100) peak remained relatively constant. This suggests that the enhanced activation at higher activation temperatures led to the collapse of interlayer structures and hence made the carbon microcrystalline structures more single-layered^{45,46}, giving rise to larger surface areas of the carbon as shown in next section. Similar relationship between the disappearance of 002 peak and surface area of carbons was also obtained by Yang et al⁴⁷.

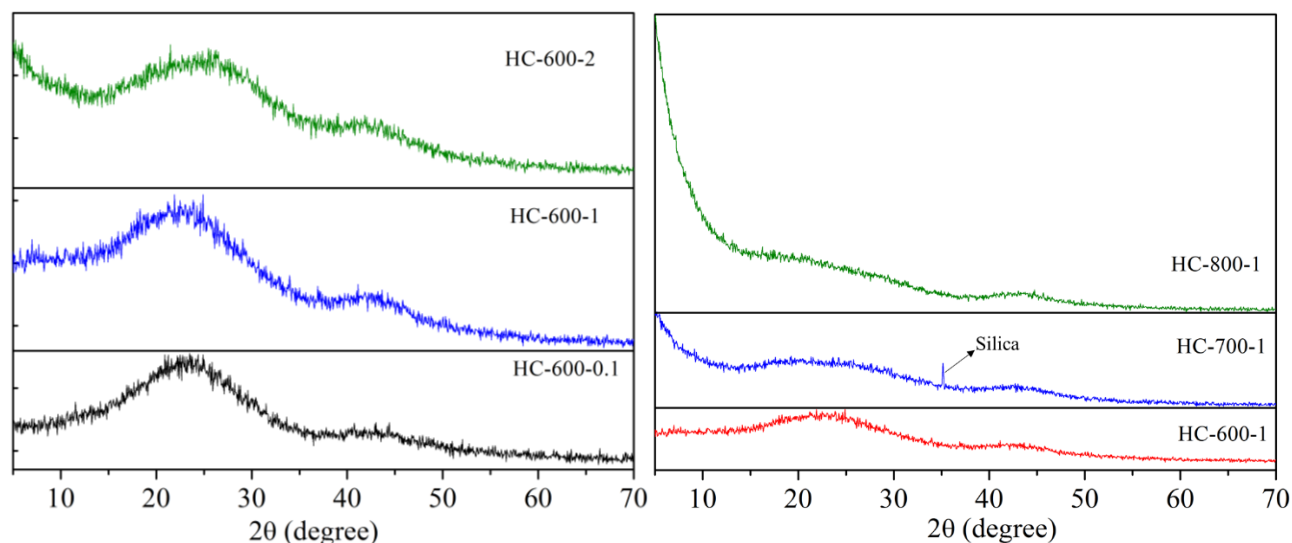


Figure 1 XRD patterns of RH carbons samples from different activation conditions

Table 1 shows the results of XRF analysis of the residual silica and potassium present in the RH carbon samples. As expected, the silicon content of the carbon decreased sharply with increasing KOH or K_2CO_3 to RH mass ratio used in the activation process, with most of the RH carbons prepared with high KOH or K_2CO_3 mass ratios (>1) having silicon contents below 2wt%. The residual silicon may occur either as unreacted silica or trapped silicates that are hard to be removed. Interestingly, the amount of potassium surviving the same excessive post-activation washing process was found to be disproportionately much larger for all the carbon samples, varying from 5 to 12 wt% which was about 3 ~ 16 times the content of silica for different samples. This sharp contrast is a strong suggestion of the different transformational pathways of the potassium present in the activating agents and the natural silica in the rice husks, and it

is believed that a significant proportion of the potassium is intercalated deep into the carbon framework formed in the activation process and is hard to be removed with the excessive washing process. Compared to our previous results reported for phenolic resin beads¹⁶, the occurrence of potassium intercalation appears to be significantly more pronounced during the chemical activation of RH carbons, being indicative of the prominent role of the RH-contained inherent silica.

Table 1 Chemical analysis by XRF of RH carbons

Sample	K, wt%	Si, wt%	Sample	K, wt%	Si, wt%
Raw	0.74	17.51	KC-600-1	13.49	5.46
HC-600-0.1	10.82	9.65	KC-700-0.1	8.47	8.86
HC-600-0.5	12.12	4.56	KC-700-1	12.35	2.44
HC-600-1	9.63	2.42	KC-700-2	4.78	1.84
HC-600-2	6.75	1.41	KC-700-3	6.74	1.75
HC-600-3	11.28	1.86	KC-800-1	7.43	1.42
HC-700-1	9.85	1.29			
HC-700-2	6.15	0.89			
HC-800-1	5.36	1.30			

3.2 Textural properties of RH-derived carbons

Fig. 2 shows the N₂ adsorption isotherms of the carbon samples prepared from the protocol of KOH activation under relatively mild conditions with the activation temperatures varying from 600 to 800 °C and RH/KOH mass ratios from as low as 0.5 to a maximum of 3. It can be seen that the adsorption isotherms of all RH-derived carbons were highly characterised by the large sharp uptake observed at low relative pressures typically < 0.1 followed by virtually horizontal plateaus at high relative pressures, this indicating the extraordinary microporosity of the RH carbons. Hysteresis at high relative pressures, which is indicative of the presence of mesoporosity, was only observed for two samples prepared from using either very low RH/KOH mass ratios or higher activation temperatures (HC-600-0.5 and HC-800-1). Compared to KOH-activated RH carbons, however, most of the K₂CO₃-activated carbons showed type IV isotherms with sloped plateaus at low relative pressures followed by variable significant amounts of hysteresis at higher relative pressures, being indicative of the wider pore size distributions ranging from micro to mesoporous structures in the K₂CO₃-activated carbons.

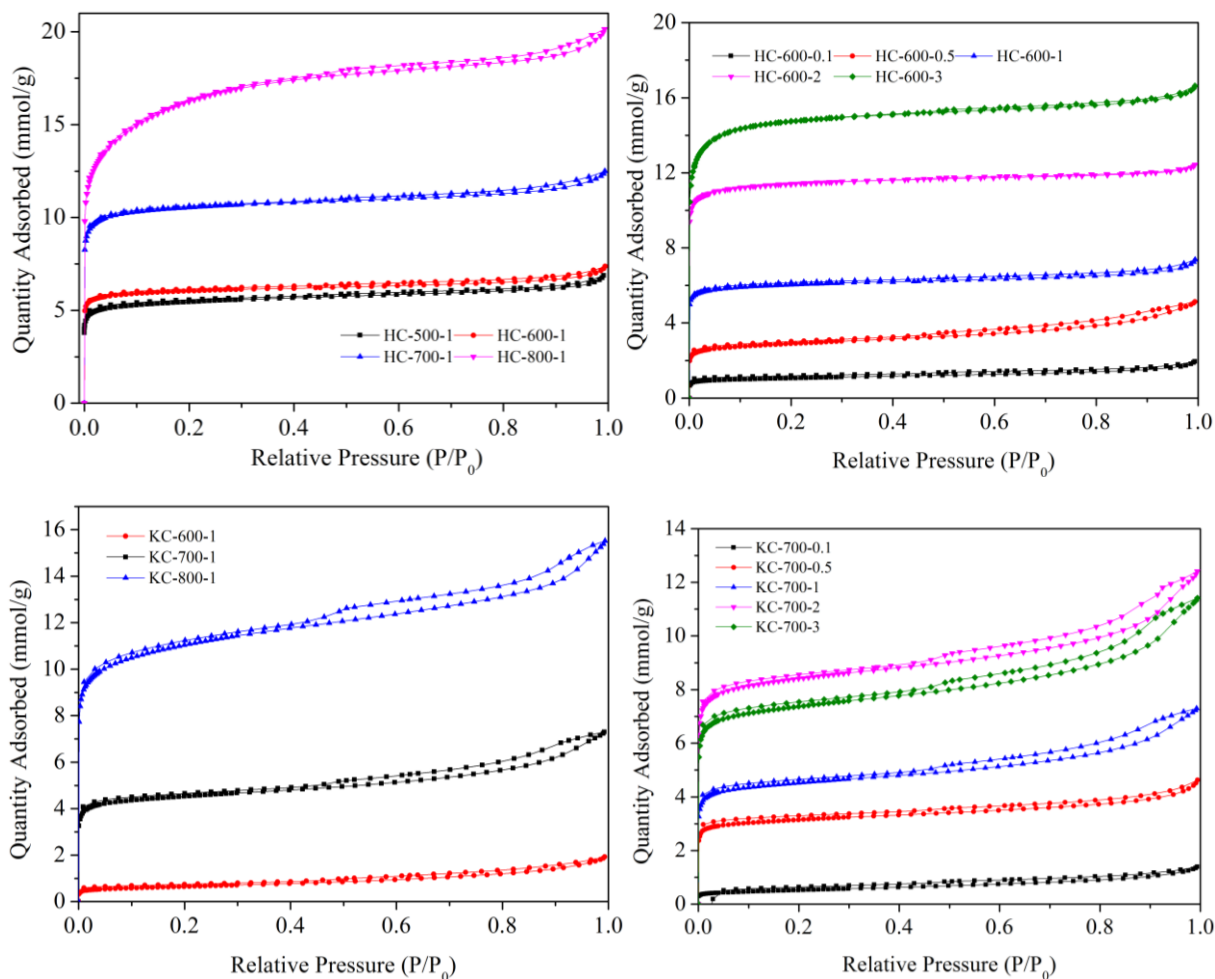


Figure 2 N₂ adsorption isotherms obtained at 77 K for RH-derived carbons from different chemical activation protocols (HC: KOH activation; KC: K₂CO₃ activation)

Table 2 summarises the surface textural parameters obtained from the BET measurements. It can be seen that the total pore volume and BET surface area increased from 0.061 to 0.64 cm³/g and 89 to 1343 m²/g, respectively when KOH/RH mass ratio increased from 0.1 to 1.0 and the activation temperature from 600 to 800 °C. It is clear that the RH-derived carbons from the protocol of KOH activation are extremely microporous, with the microporosity accounting for up to 95% of the total porosity. More importantly, the microporosity of the RH carbons, as shown in Fig. 3, was found to consist mostly of ultra-micropores with pore diameters centred on 0.36 and 0.55 nm, which represents 84% of total microporosity for the carbon sample prepared at 600 °C with a KOH/RH mass ratio of 1. Such well-defined ultra-microporosity with extremely narrow pore size distributions obtained for the RH carbons can usually only be achieved with some special metal organic frameworks (MOFs) built from a single small ligand⁴⁸ and the carbons derived from carefully selected costly precursors and using cumbersome methodologies⁴⁹.

Table 2 Specific surface areas, pore structure parameters of the bio-carbons

Sample	S_{BET} (m^2/g)	V_{total} (cm^3/g)	V_{micro} (cm^3/g)	$V_{micro<1nm}$ (cm^3/g)	$V_{micro<1nm}/V_{micro}$	V_{micro}/V_{total}
<i>KOH-activated carbon</i>						
HC-600-0.1	89	0.061	0.029	0.018	62%	48%
HC-600-0.5	249	0.16	0.083	0.057	69%	52 %
HC-600-1	536	0.24	0.19	0.16	84%	79 %
HC-600-2	1025	0.43	0.39	0.30	81%	95 %
HC-600-3	1303	0.52	0.47	0.34	72%	90 %
HC-700-1	976	0.39	0.33	0.26	79%	85 %
HC-700-2	1197	0.47	0.43	0.33	77%	91 %
HC-800-1	1343	0.64	0.49	0.30	61%	77 %
<i>K₂CO₃-activated carbon</i>						
KC-700-0.1	42	0.044	0.012	0.006	50%	27 %
KC-700-0.5	274	0.15	0.10	0.072	72%	67 %
KC-700-1	395	0.24	0.14	0.094	67%	58 %
KC-700-2	640	0.38	0.23	0.17	74%	61 %
KC-700-3	741	0.39	0.25	0.19	76%	64 %
KC-800-1	944	0.60	0.37	0.24	65%	62%

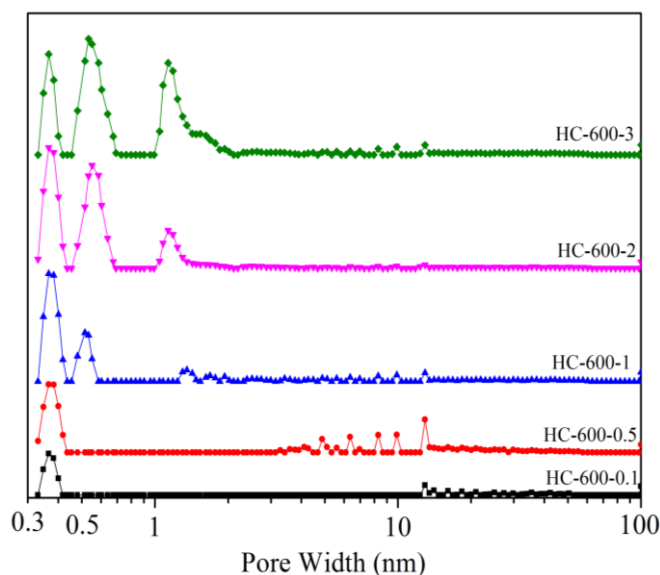
**Figure 3 NLDFT pore size distributions for RH samples from KOH activation with different KOH/RH mass ratios at 600 °C**

Figure 4 shows the effect of activation temperature and KOH/RH mass ratio on the development of ultra-microporosity. It can be seen that the volume of ultra-micropores increased both with the activation temperature and KOH/RH mass ratio, indicating an enhanced activation effect. However, at a given KOH/RH mass ratio, the ultra-micropore volume as a fraction of the total micropore volume decreased with activation temperature whereas at a given activation temperature, the percentage of ultra-

microporosity was found to decrease with an increase in KOH/RH ratio up to 3.0. The decrease in the relative ultra-microporosity with increasing severity of activation conditions was believed to be associated with the formation of increasingly larger micropores with a broader size distribution, with mesoporosity starting to emerge when the activation temperature was higher than 700°C (sample HC-700-1) as shown in Fig. 2.

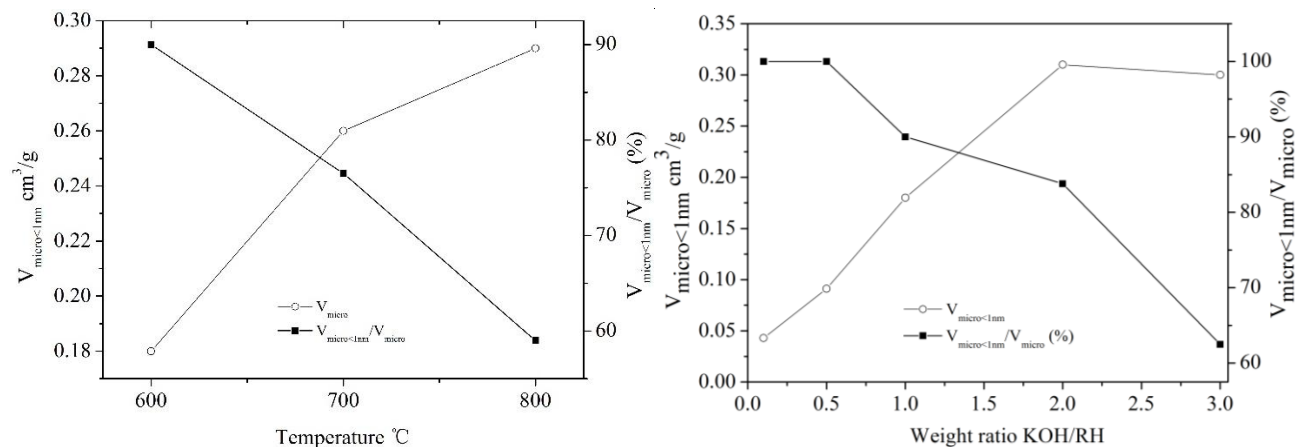
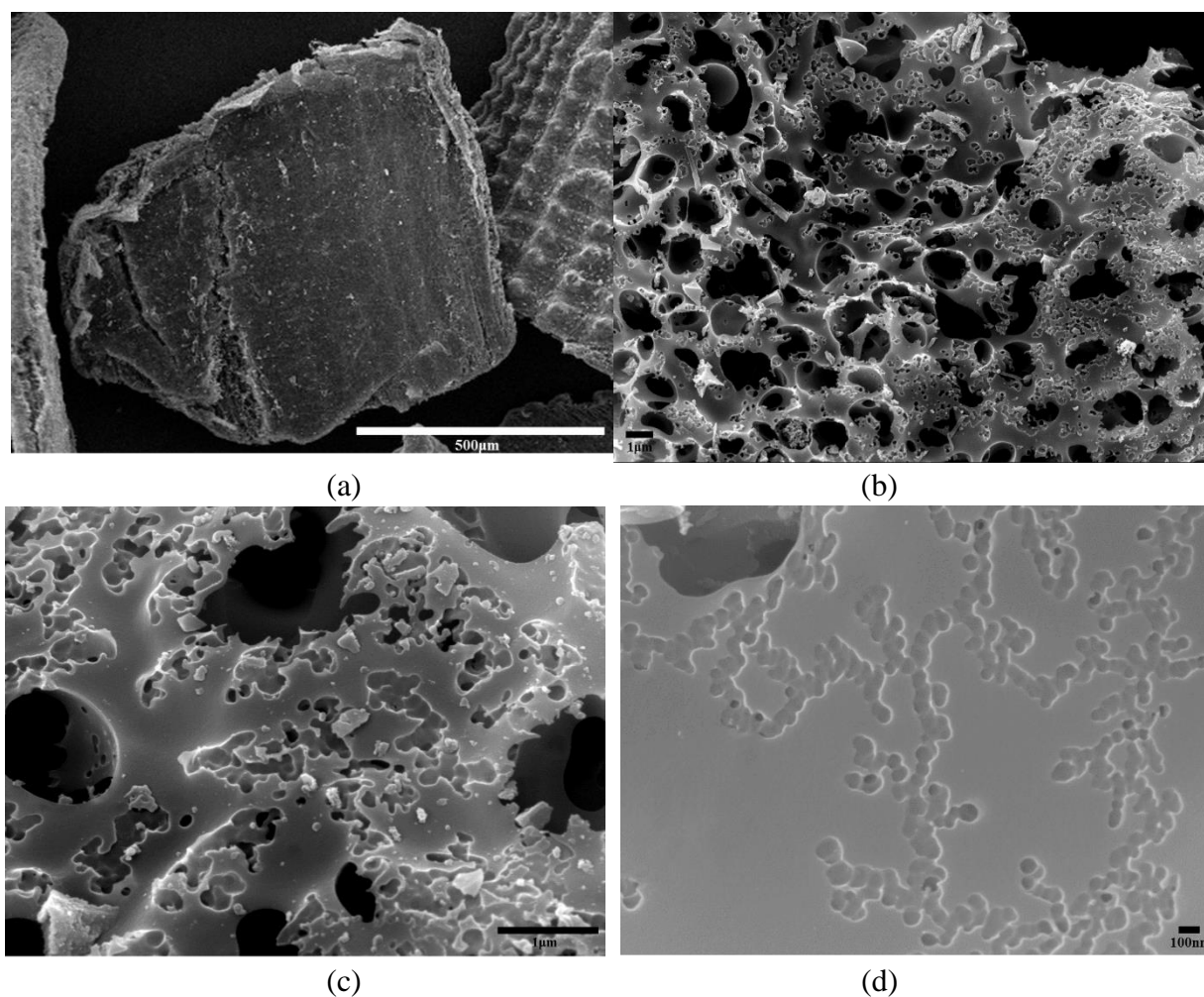


Figure 4 Effect of activation temperatures and KOH/RH mass ratios on ultra-microporosity of KOH-activated RH carbons

Compared to the KOH activation, the results shown in Table 2 and Fig.2 show that the RH carbons from the one-step K_2CO_3 activation, which can be considered as part of KOH activation but can only take place at higher temperatures, were found to be significantly less microporous owing to the formation of mesoporosity that appears to become more pronounced with increasing activation temperatures. The highest surface area was obtained at only $944 \text{ m}^2/\text{g}$ for the sample prepared at the highest K_2CO_3 activation temperature (800 °C) investigated. However, it is noteworthy that despite the smaller ultra-micropore volumes, the relative ultra-microporosities of the K_2CO_3 -activated RH carbons were overall comparable to those of the carbons from the one-step KOH activation under similar conditions, suggesting that the RH carbons obtained with K_2CO_3 activation essentially exhibit a distinct bimodal pore structure consisting mainly of two groups of porous structures, namely the mesopores and the ultra-micropores below 1 nm in diameter. However, as K_2CO_3 activation appears to favour the formation of mesoporosity at a cost of microporosity, it can be reasonably envisaged that the RH carbons obtained

with K_2CO_3 activation will become increasingly mesoporous with increasing activation temperatures and/or K_2CO_3 /RH mass ratios, eventually leading to the formation of mesoporous RH carbons ⁴⁹.

Figure 5 illustrates the SEM images of the raw RH and its derived carbon samples from KOH and K_2CO_3 activations. It can be seen that despite the lower activation temperature used, the carbon sample from the KOH activation shows a much more developed porous structure than the K_2CO_3 -activated carbons, being consistent with the above results obtained. In order to further understand the microporous structure of HC-600-1, transmission electron microscopic (TEM) imaging analysis were also performed. As shown in Figure 5(f, g), slit-like ultra-micropores can be clearly seen in the TEM images and the ultra-microporosity distributed across the porous network skeleton.



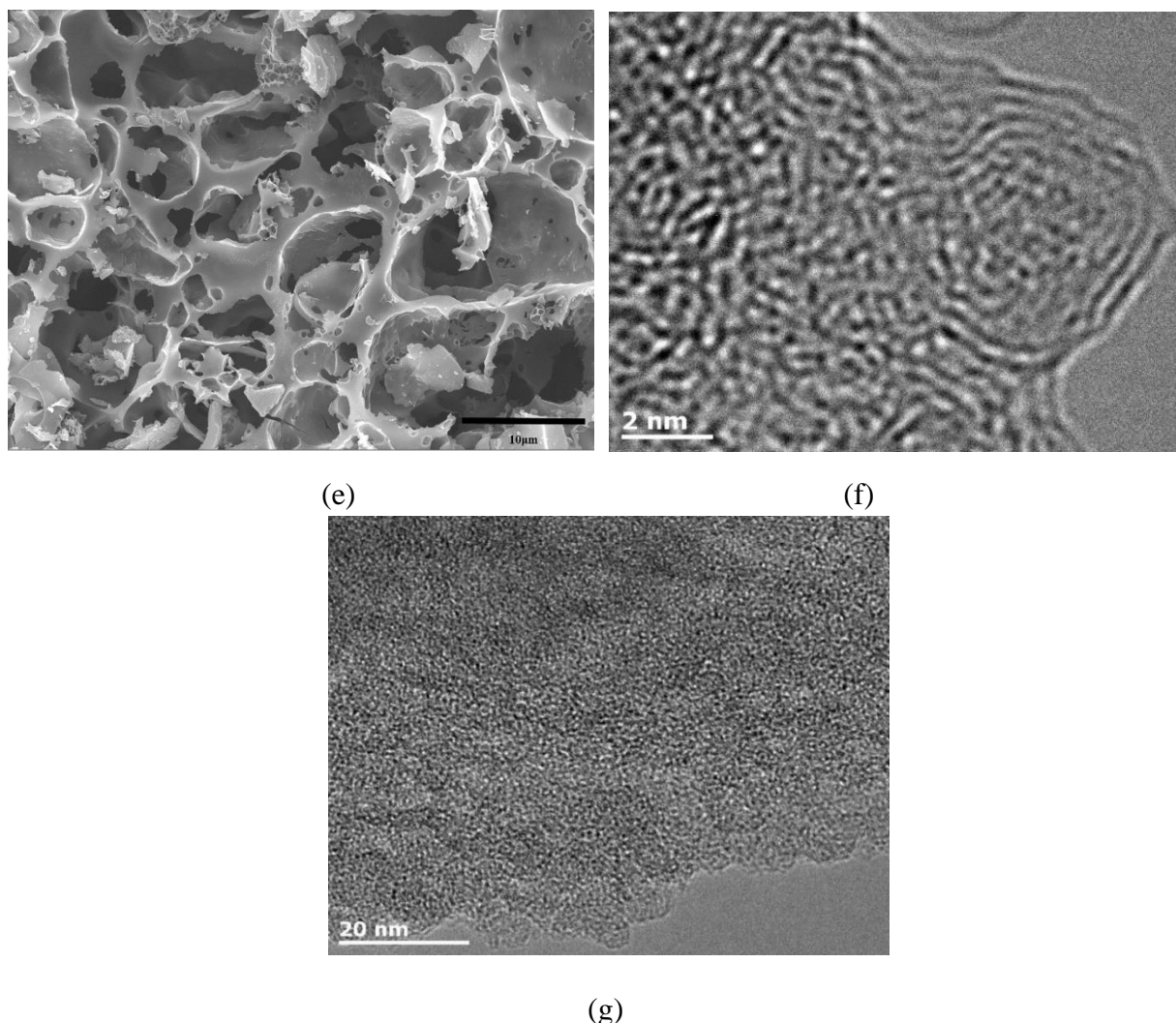
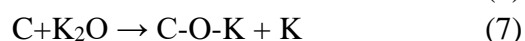
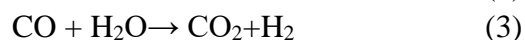
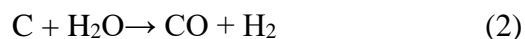


Figure 5 SEM images of raw RH (a) and its derived carbons from KOH and K₂CO₃ activation (HC-600-1 (b)-(c); KC-700-1(d)-(e)) and TEM images of sample HC6001 (f)-(g)

3.3 The role of RH inherently contained silicon in ultra-microporosity development

The formation of well-defined ultra-microporosity at such exceptionally high levels, which has never been observed for any other carbon materials prepared with similar methodologies⁵⁰, is highly suggestive of other reactive element(s) involved during the activation. RH is well known for its uniquely high contents of silica (15–23 wt%) present in an inherent structural framework at molecular levels and some of the silicon species are even chemically bonded to the functional groups of the carbonaceous rice husk^{51, 52}. During chemical activation, these inherently present silicon species within the framework of rice hulls can play a prominent in-situ template role in the development of the exceptionally high levels of ultra-microporosity observed for the RH carbons.

Previous investigations have revealed that KOH activation of carbonaceous materials for activated carbon production involves the following major chemical reactions (1) to (8) ⁵³⁻⁵⁶ whereas K₂CO₃ activation only involves the reactions (5) to (8) and requires higher temperatures to achieve high levels of activations⁵⁷⁻⁵⁹. The significance of individual reactions and hence the porous structures of resultant activated carbons are determined by both the activation temperature and the amount of KOH used. In general, activation efficiency increases with increasing KOH/carbon ratio and activation temperature in particular, due to the enhanced chemical reactions and associated pore creating and widening effect. It is noteworthy that the pore widening effect accelerates significantly with increasing activation temperatures, because of the higher kinetic energy possessed by the melt of K₂CO₃, K₂O and the vapour of metallic potassium at higher temperatures.



In general, the results obtained for the RH carbons agree well with previous findings. However, compared to other biomass feedstocks free of silica, the following additional pore-creating reactions (9~11) between the activating agents and RH-contained silica also take place with varying significance, which provide additional activation as the water-soluble silicates formed can easily be removed to free the porosity during the washing process. The results present in Table 1 confirm the removal of silicon as a result of the additional reactions during the chemical activation process.



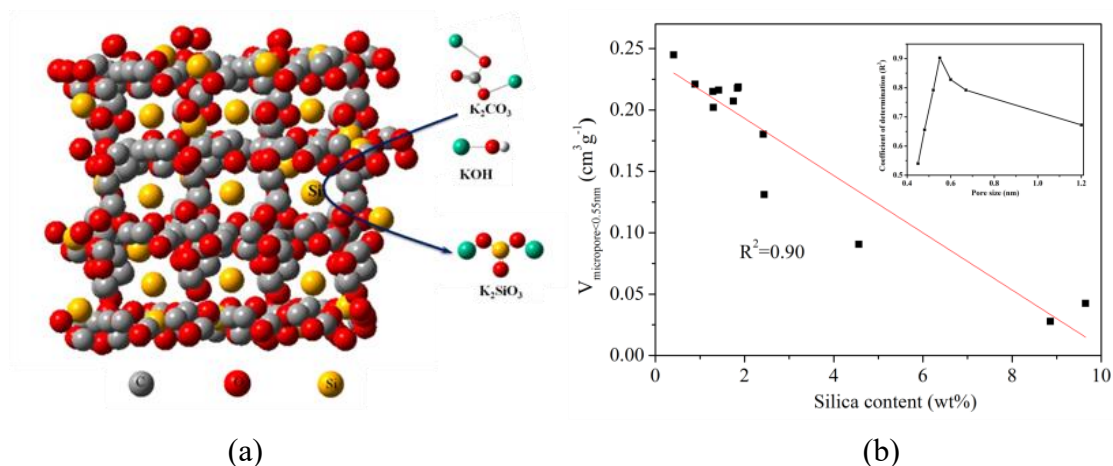


Figure 6 Schematic diagram for the silicon-containing RH framework and the pore-creating reactions of silicon with activating agents (a) and the relationship between the ultra-micropore volume and the residual silicon content of the carbons (b)

These additional reactions were believed to be the main factors responsible for the extraordinary ultra-microporous structures observed for the RH carbons, given the inherent nano-scale distribution of the natural templating silica within the matrix of rice husk⁶⁰. It is also reasonable to assume that the formation of silicates may also help retain the resultant ultra-microporosity by weakening the pore widening effect of further carbon reactions with the activating agents. Indeed, a linear relationship as shown in Fig. 6(b) was observed between the volume of ultra-micropores (<0.55nm) and the residual silicon contents of the RH carbons (Table 2), showing that the micropore (<0.55nm) volume increases with the increasing removal of residual silicon in the form of potassium silicates.

3.4 CO₂ adsorption properties of RH carbons

3.4.1 Static adsorption measurement

Fig. 7 shows the adsorption isotherms at 0 and 25 °C for the RH carbons prepared from the one-step carbonisation–activation with KOH under different conditions. Clearly, the CO₂ uptake of the RH carbons was affected substantially by both the activation temperature and the amount of activating agent used. At the given activation temperature of 600 °C, the results shown in Fig. 7(a, b) indicate that on increasing the KOH/RH mass ratio from 0.1 to 2, the CO₂ adsorption capacity increased sharply from 2.35 and 1.88 mmol/g to 4.75 and 5.91 mmol/g at 0 and 25 °C and 1 bar CO₂ respectively, being consistent with the increased activation efficiency and removal of RH-contained silica as shown in Table 2.

However, a further increase in KOH/RH ratio from 2:1 to 3:1 resulted in a significant decrease in CO₂ uptake from 4.75 to 4.1mmol/g at 25°C and 1 bar, despite the continuous increase in the porosity but clearly at a cost of ultra-microporosity as a result of enhanced pore widening effect (Table 2). A similar trend was also observed for the effect of carbonisation and activation temperature (Fig. 7c) on CO₂ uptake, with the carbons prepared at 600 and 700 °C showing the best adsorption performance in general. Of all the KOH-activated samples, the RH carbon (HC-600-2) prepared at 600 °C with a KOH/RH ratio of 2:1 exhibited the highest adsorption capacities of 5.91 and 4.75 mmol/g at 1 bar, and 2.96 and 2.0mmol/g at 0.15 bar CO₂ at the adsorption temperatures of 0 and 25 °C, respectively. A comparison with other materials (Table S1) shows that the extraordinary CO₂ uptakes of the RH carbons of this study at low CO₂ partial pressures represent the one of the highest capacities ever reported for any carbon materials which are usually prepared from cost-prohibitive precursors and sophisticated methodologies, and exceed the performance of most MOF materials for post-combustion CO₂ capture. Compared to KOH activation, however, the carbons obtained from the integrated carbonisation and K₂CO₃ activation process appear to be generally less effective in adsorbing CO₂ (Fig. 8), with the sample prepared at 800 °C (KC-800-1) showing the highest CO₂ uptakes of 2.3 and 4.8 mmol/g at 0 °C and CO₂ partial pressures of 0.15 and 1 bar CO₂, respectively.

For both KOH and K₂CO₃ activations, the adsorption isotherms also show that samples prepared in relatively mild conditions often showed higher CO₂ uptake capacities at low CO₂ partial pressures up to 0.2 bar but exhibited lower capacities in the higher pressure region, compared to the samples prepared in less mild activation conditions (e.g. HC-600-1 vs HC-600-3; HC-600-1 vs HC-700-2 and HC-800-1; and KC-700-1 vs KC-800-1), highlighting the differential effect of the surface textural and chemical properties on CO₂ uptake and related adsorption mechanisms at different partial pressures.

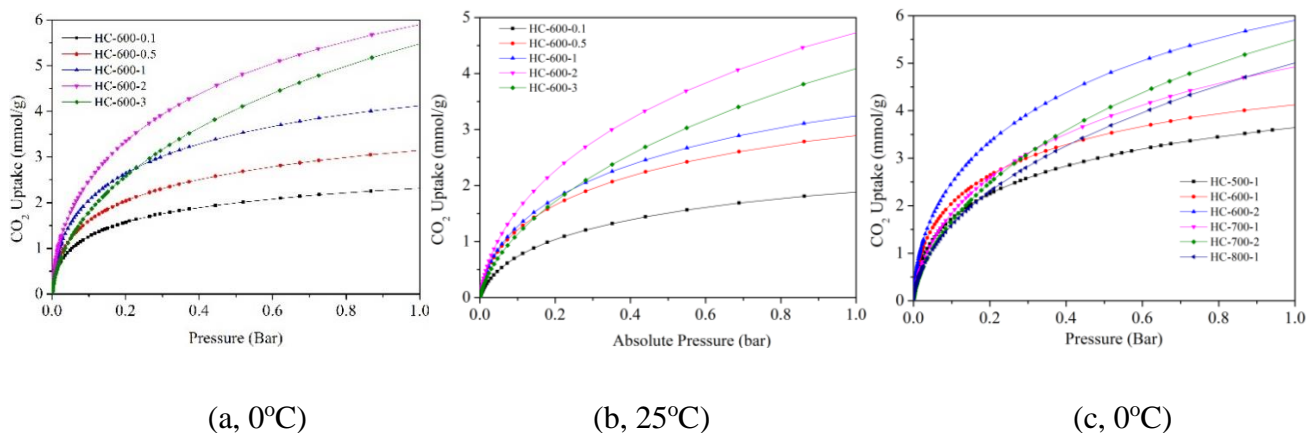


Figure 7 CO₂ adsorption profiles at 0 and 25 °C for RH carbons from the one-step carbonization-activation with KOH under different conditions. (a), (b): adsorption isotherms at 0 and 25 °C, respectively, (c), adsorption isotherms at 0 °C for carbons from different carbonization/activation temperatures.

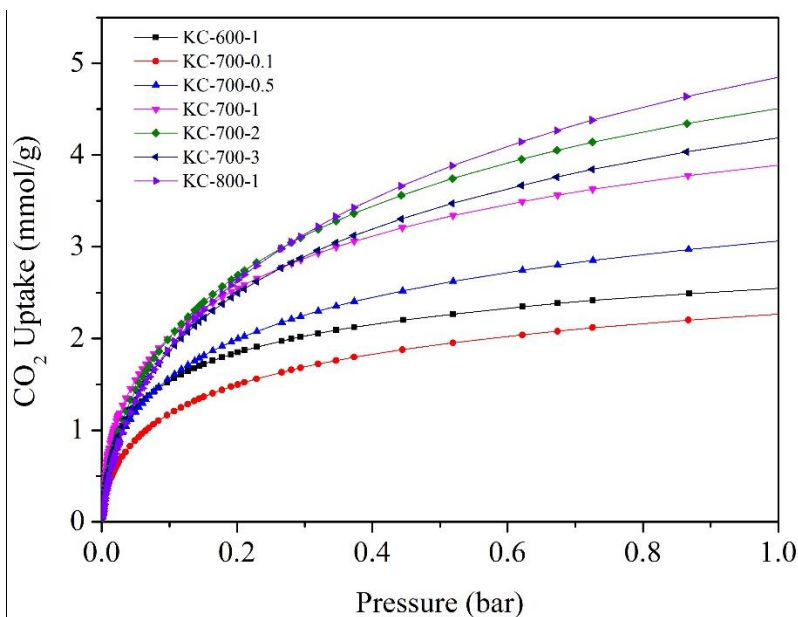


Fig. 8 CO₂ adsorption profiles at 0 °C for the RH carbons from the carbonization-activation scheme with K₂CO₃ as the activating agent under different conditions

3.4.2 Dynamic adsorption and cyclic adsorption/desorption measurement

Fig. 9 shows the adsorption characteristics and the cyclic adsorption/desorption performance for selected samples, obtained from TGA at 25 °C and 0.15 bar CO₂ (N₂ balance). As shown in Fig. 9a, all the RH carbon samples demonstrate fast CO₂ uptake in the simulated flue gas stream under the dynamic TGA conditions, with their achieved equilibrium adsorption capacities being essentially identical to those obtained under the static BET measurement conditions (Fig. 7b). A remarkable equilibrium uptake capacity of 2.0 mmol/g was obtained with the best-performing HC-600-2 sample and 90% of the

equilibrium capacity was achieved in less than 2 minutes (Fig.9a), while its stable and excellent reversible adsorption performance was demonstrated by the cyclic life-time performance test results (Fig.9b). It is also worth mentioning that the least activated HC-600-0.1 sample, which has a surface area of only 89 m²/g and a micropore volume of 0.029 cm³/g, still achieved an impressive adsorption capacity of 1.3 mmol/g, and this may indicate the extraordinary role of the potentially unique surface chemistry of the RH carbons that has rarely been seen for any other carbon materials. The above results highlight the high adsorption capacity and desirable fast adsorption kinetics of the rice husk derived carbons of this study.

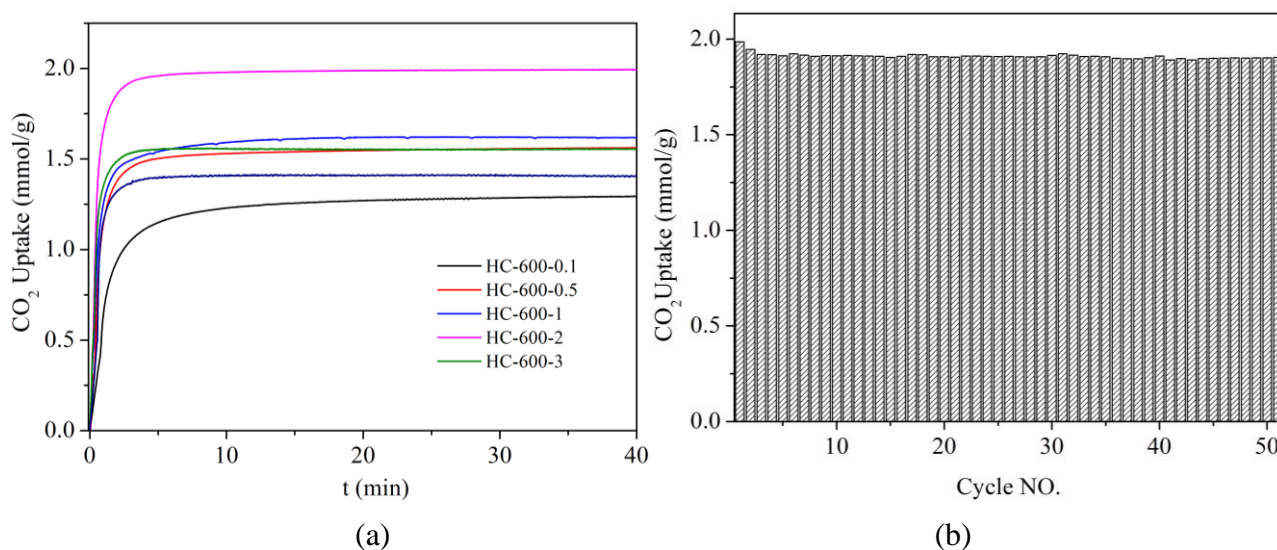


Figure 9 (a) the isothermal adsorption curve of selected RH carbons; (b) the cyclic adsorption/desorption performance of the best-performing HC-600-2 sample: both under simulated flue gas conditions of 15% CO₂ and 85% N₂ at 25 °C for adsorption and 120 °C for desorption in N₂

3.5 The role of surface textural and chemical properties on CO₂ adsorption

The CO₂ uptake performance of the RH carbons prepared in different carbonisation and activation conditions appears to have no direct links with the general surface textural properties as shown in Table 2 and Fig. 2. For instance, the sample HC-800-1, which had the largest surface area of 1343 m²/g with a total volume of 0.64 cm³/g (Table 2), had the lowest CO₂ uptakes of only 1.96mmol/g at 0°C and 0.15 bar CO₂, while the sample HC-600-2 with a considerably lower surface area of 1025 m²/g and total pore volume of 0.43 cm³/g had the remarkably higher capacity of 2.96mmol/g and the sample HC-500-1, which had the smallest surface area of only 470 m²/g and total pore volume of 0.22 cm³/g, had the

capacity of 2.05mmol/gat 0 °C and 0.15 bar CO₂. These results strongly suggest the unique pore size distributions of the samples can be more relevant to the CO₂ uptake capacities.

Further examinations as shown in Fig.10 indicate that the CO₂ capture capacity of the RH carbons at the different adsorption temperatures and CO₂ partial pressures investigated is indeed only directly proportional to the volume of micropores smaller than 1 nm. Therefore, carbonisation and activation conditions leading to widened porous structures at a cost of fine microporosity (Table 2) will result in a decrease in CO₂ uptake despite the induced further increase in surface area or total pore volume. At a CO₂ partial pressure of 0.15 bar, the CO₂ uptake capacity at 0 °C was found to be almost linear with the volume of micropores smaller than 0.5 nm, with a high correlation coefficient (R^2) of 0.90 (Fig. 10a). Similar linear relationships were also obtained at other adsorption temperatures and pressures, while the unique pore size giving rise to the best correlation increased to 0.60 nm at 0 °C and 1 bar (Fig. 10b, $R^2 = 0.98$) but decreased significantly to 0.44 nm when adsorption took place at 25 °C and 0.15 bar CO₂ (Fig. 9c, $R^2 = 0.92$), respectively. It was also found that the coefficient of determination (R^2) decreased sharply even with a slight increase in the pore sizes identified (Fig. 10d). It is well known that smaller micropores have higher adsorption potentials as a result of the superposition of the stronger van der Waals force produced by the adjacent walls of smaller micropores. While the above results further confirm the vital role of ultra-microporosity (< 1nm) on the CO₂ uptake, they are also highly suggestive of the existence of a critical pore size distribution that essentially determines the overall CO₂ uptake performance at specific adsorption temperatures and pressures, with the critical pore size decreasing with increasing adsorption temperature and/or decreasing CO₂ partial pressure.

The relation between the CO₂ uptake and pore size obtained for the RH carbons agrees well in general with previous research findings that the CO₂ adsorption capacity of carbon materials is mainly associated with the volume of the pores smaller than a specific pore size determined by the adsorption pressure and temperature^{19, 61}. However, it is obvious that the surface textural properties alone cannot account for the extraordinary CO₂ uptakes of the RH carbons, as clearly shown by the exceedingly large y-axis intercepts of the above linear relations that were never observed before.

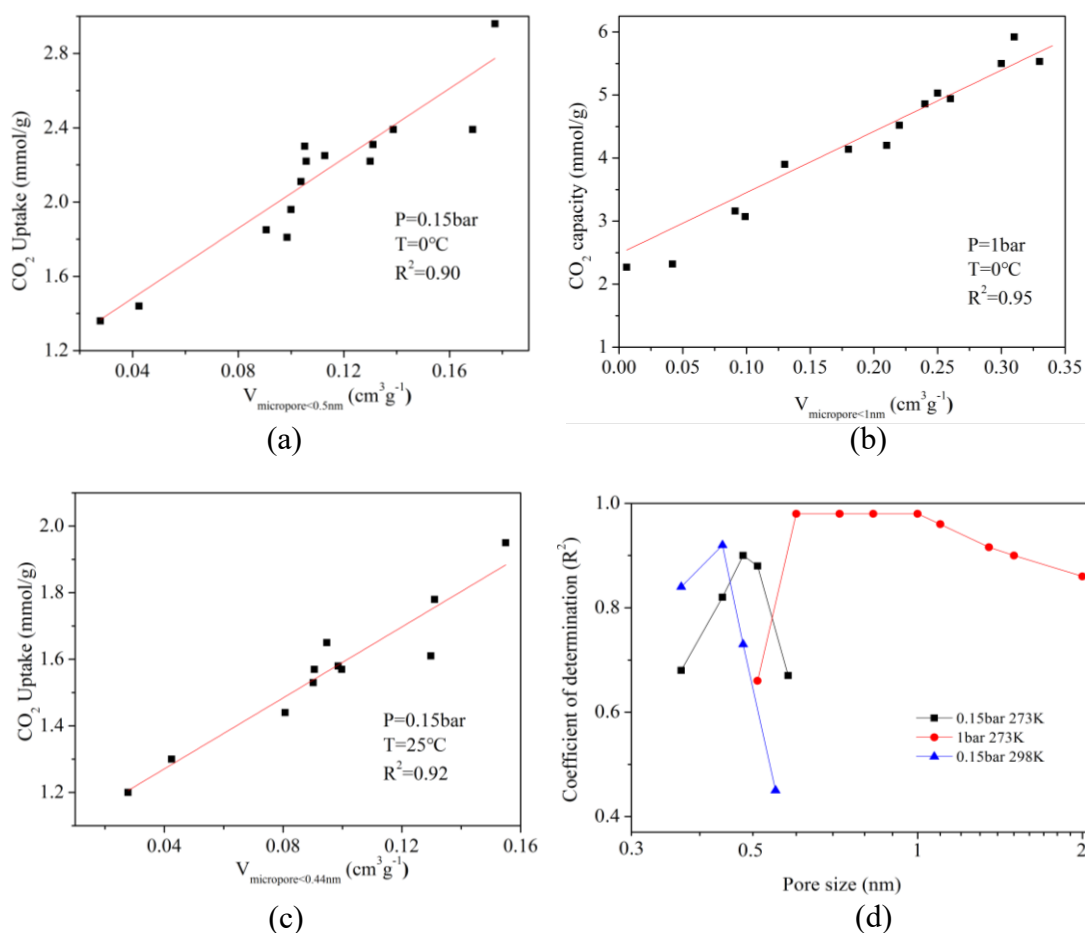


Figure 10 Relationship between CO₂ uptake and ultra-micropore volume of RH carbons: (a) 0 °C, 0.15 bar CO₂; (b) 0 °C, 1 bar; (c) 25 °C, 0.15 bar CO₂; (d) the change of coefficient of determination R^2 with the increase of pore size

At 0.15 bar CO₂, the value of intercept derived from linear extrapolation, which characterises the relative significance of surface chemical properties in CO₂ adsorption, was obtained as 1.11 mmol/g at 0 °C and 1.00 mmol/g at 25 °C. For sample HC-600-2, this represents 37% and 50% of its CO₂ uptake capacity at 0 °C and 25 °C and a CO₂ pressure of 0.15 bar, respectively. At 0 °C and 1 bar CO₂, the intercept increased to 1.89 mmol/g, accounting for 32% of the adsorption capacity of HC-600-2. Clearly, the relative role of surface chemistry in CO₂ adsorption is even more significant for all other samples where the CO₂ uptake is lower due to smaller ultra-microporosity. The use of surface modification via various methodologies as a means to boost the adsorption capacity of carbon materials has been the focus of many investigations over recent years, but with limited improvements being achieved as shown in Table S1. The remarkable relative contribution of surface chemistry as characterised by the large intercept obtained for the RH carbons has never been observed in previous investigations where the intercept of similar relationships

was found to be near zero while the conclusions on the role of surface chemistry were often ambiguous or contradictory^{19, 46, 61, 62}.

As the RH carbon is virtually nitrogen-free, it is believed that the excess adsorption capacity of the RH carbons was linked with the presence of extra framework metal (K^+) cations that were formed as a result of potassium intercalation achieved during the KOH activation or K_2CO_3 activation¹⁶. It has been well known that extra-framework cations usually present in zeolitic materials can form strong local electric fields that can polarise adsorbate molecules and hence provide either additional active adsorption sites and/or enhance the interaction of the adsorbate with the adsorption surface, with the magnitude of the effect determined by both the charge density of the extra-framework ions and the electric quadrupole of adsorbate^{16, 63-65}. CO_2 has a very large electrical quadrupole moment, which is over three times higher than that of N_2 ($-1.43 \pm 0.06 \times 10^{-39} \text{ Cm}^2$ vs $-4.65 \pm 0.08 \times 10^{-40} \text{ Cm}^2$)⁶⁶, implying that CO_2 molecules can be preferentially polarised in an electrostatic field. Therefore, the large excess CO_2 adsorption capacity of the RH carbons, which could not possibly be accounted for by their surface textural properties, could be presumably owing to the strong preferential CO_2 polarisation by the extra-frame work K^+ ions present in the framework of the RH carbons. It has been well established that CO_2 polarisation in zeolitic materials gives rise to the formation of various adsorption complexes, which range from bridged and unbridged complexes with single and dual exposed ions to bent carbonate-like species, the latter also involving the participation of both the exposed ions and a lattice oxygen^{64, 67}. The great excess adsorption capacity or the large y-axis intercepts observed for the RH carbons (Fig. 10) are clearly attributable to the similar adsorption complexes formed via the similar adsorption mechanisms. It appears that the presence of extra-framework K^+ ions particularly benefit the CO_2 adsorption at high adsorption temperatures or low partial pressures, with its contribution to the overall CO_2 uptake increased from ca. 37% to 50% when adsorption temperature increased from 0 °C to 25 °C at 0.15 bar and from 32% to 37% when CO_2 pressure decreased from 1 to 0.15 bar at 0 °C.

Presumably, the formation of extra framework cations (K^+) is particularly associated with the potassium intercalated into the carbon network structures during activation, with the degree of potassium intercalation and hence the density of the extra-framework ions determined by the activation conditions and resultant textural properties of the carbons¹⁶. The above results suggest that the formation of extra-

framework ions was considerably enhanced in the RH carbons, potentially due to their exceedingly high ultra-microporosity that may expectedly either increase potassium intercalation or stabilise the derived extra-framework ions.

The SEM-EDX element mapping obtained for the sample HC-600-2 (Fig. 11a) reveals the extensive uniform spatial distribution of the intercalated potassium species at microscopic scales, which is indicative of its high surface polarity, while the characterisations by XPS (Fig. 11b) demonstrates the presence of potassium, silicon, aluminium and calcium at varying quantities in different forms of zeolitic structures. The K2p spectrum for the potassium in the sample HC-600-2 exhibited two peaks at 293.2 and 296.0eV with an intensity ratio of 2:1 and a difference in binding energy of 2.8 eV, which are characteristic of the spin-orbit-split doublet ($K2p_{3/2}$ and $K2p_{1/2}$) of surface potassium cations and oxides^{68, 69} rather than carbonate species, which usually have their $K2p_{3/2}$ peak at 292.2 eV⁷⁰. Given the significantly enhanced and fully reversible CO₂ adsorption, this suggests the formation of strongly bound potassium surface complexes presumably in the form of $O^{\delta-}-K^{\delta+}$ and/or extra-framework K^+ cations. The residual silicon compounds, which survived the excessive post-activation washing, have a Si2p spectrum comprising two peaks at the binding energies of 102.6eV and 103.8eV, which is indicative of the existence of X-type zeolitic structures⁷¹ and SiO₂⁷², respectively. The XPS characterization also indicates the presence of trace quantities of alumina, which had an Al2p peak at 74.6 eV that indicates the presence of X and/or Y-type zeolites⁷¹, and calcium species showing two Ca2p peaks at 351.2 and 347.7eV, which are suggestive of the existence of CaCO₃⁷³ and A-type zeolitic structures^{64,74}, respectively. XRF analysis conducted for sample HC-600-2 shows that sample contained 0.15 wt% Al, 0.57 wt% Ca in addition to K and Si, confirming the existence of trace quantities of Al and Ca bearing species. Given the unique distribution of silicon compounds in rice husk at molecular levels, the above results may reveal that part of the rice husk-contained silicon was transformed to different forms of zeolitic structures incorporated into the carbon networks, which essentially transformed the RH carbons to a type of zeolite-carbon nanocomposite materials, whereas the alkali-metal zeolite structures are well known for the abundance of extra-framework cations responsible for their usually strong surface affinity to CO₂⁶⁴.

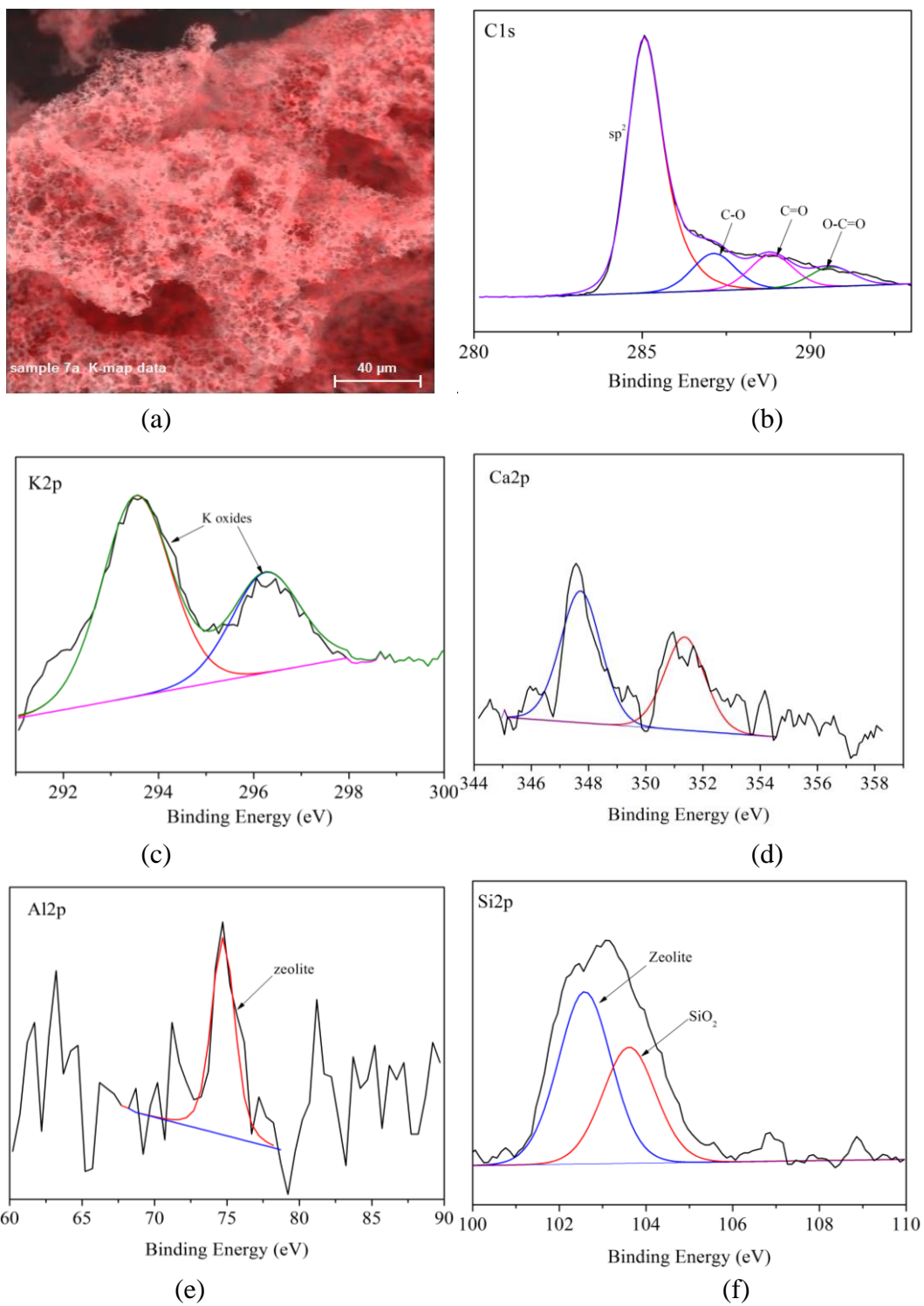


Figure 11 (a) SEM-EDX element mapping showing the spatial distribution of potassium in HC-600-2; (b)-(f) XPS spectra of the major heteroatoms identified in HC-600-2

3.6 Heat of CO₂ adsorption of RH carbons

The heat or enthalpy of adsorption is an important parameter to indicate the surface affinity of an adsorbent toward CO₂ and hence reflect the strength of their interaction. Ideally, a suitable adsorbent for CO₂ capture should have a moderate heat of adsorption to facilitate high CO₂ uptakes at low CO₂ partial pressures and/or reasonable flue gas temperatures without energy-intensive flue gas deep cooling. This is because too high a heat of adsorption can lead to increased energy requirement for CO₂ desorption or sorbent regeneration whilst if the heat of adsorption of a sorbent is too low (e.g. those of typical commercial carbons^{17, 19, 49, 75}), the sorbent will give rise to unacceptably low CO₂ uptakes at typical flue gas temperatures and CO₂ partial pressures. Fig. 12 shows the heat of CO₂ adsorption measured by TG-DSC at 25 °C and a CO₂ partial pressure of 0.15 bar in N₂ for a selection of RH carbon samples. The heat of adsorption for the RH carbons ranged from 32 to 38.4 kJ/mol and showed a decrease with increasing activation temperature and the ratio of KOH or K₂CO₃ to RH (Fig. 12a), which corresponds well to the increased porosity development and hence the increased role of surface textural properties in adsorption. Though the measured adsorption heat by TG-DSC for the RH carbon represents the average heat of adsorption rather than the isosteric heat of adsorption used in prior studies, which is a function of surface coverage and usually calculated from using adsorption isotherms, they are still considerably higher than those reported for zeolite⁷⁶ and most MOFs⁷⁷⁻⁷⁸ and virtually any other carbon materials^{17, 19, 49} (e.g. Maxsorb and Norit R1 Extra (red bar), 17-25kJ/mol¹⁷), being indicative of the strong interaction of the adsorbed CO₂ phase with the surface. The observed strong linear increase of adsorption heat with increase in the content of intercalated potassium (Fig. 12b) confirms the significance of potassium intercalation in modifying the carbon surface chemistry via the formation of highly polarising extra-framework K^{+δ} ions or zwitterion-like structures. As shown in Fig. 12a and Table 2, the fact that the least activated samples prepared under the mildest activation conditions (e.g. HC-600-0.1, HC-600-0.5 and KC-600-1) was found to have the highest heat of adsorption further reflects the strong surface inhomogeneity of the potassium-intercalated RH carbons with incorporated zeolitic structures as revealed in Fig. 11. Further, compared to previous findings^{17, 19, 49}, the large y-intercept of ca. 28kJ/mol derived from the linear relationship (Fig. 12b), presumably attributable to the non-electrostatic interactions, also suggests that

the micropore filling/capillary condensation in the RH carbons could be significantly enhanced or the micropores filled to a higher degree due to the extended effect of strong surface electrostatic forcing.

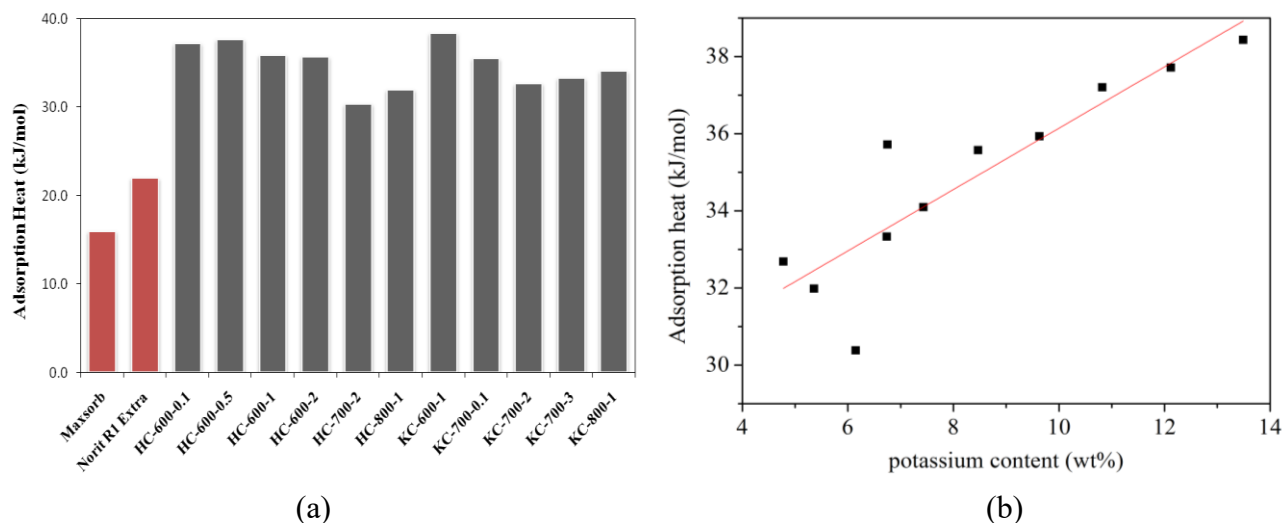


Figure 12 (a) Specific heat of CO₂ adsorption measured by TG-DSC (flue gases: 15% CO₂ + 85% N₂; adsorption temperature: 25 °C); (b) the relationship between K content and adsorption heat.

4 Conclusions

Novel activated carbons with exceedingly high ultra-microporosity and strongly modified surface chemistry in favour of CO₂ adsorption were prepared from the abundant agricultural waste of rich husk, using a facile approach that essentially integrated the carbonisation and simultaneous activation into a single one-step process. The synthesized bio-carbons have showed exceedingly high levels of ultra-microporosity, owing to the unique templating role of the natural silicon species contained within the RH molecular framework structures. A combination of high ultra-microporosity and unique surface chemistries led to remarkable CO₂ uptake capacities of up to 5.91 mmol/g at 0 °C and 1.0 bar and 2.0 mmol/g at 25 °C and a CO₂ partial pressure of 0.15 bar, which represent one of the highest CO₂ uptakes ever reported for designer carbon and MOF materials. Taken with the exceptionally high heat of adsorption, the unusually prominent role of surface chemistry in CO₂ adsorption, which was responsible for up to 50% of total CO₂ uptake, were highly indicative of the significantly enhanced formation of extra-framework potassium ions leading to the extraordinary surface affinity to CO₂ observed for the RH carbons.

Characterisations by XPS and EDX elemental have demonstrated the extensive uniform spatial distribution of the intercalated potassium at microscopic scales and the existence of various types of zeolitic aluminosilicate structures incorporated into the RH carbon frameworks, which essentially transformed the carbons into potassium-intercalated zeolite-carbon composite materials.

ASSOCIATED CONTENT

Supporting information

The Supporting Information is available free of charge on the ACS Publications website

AUTHOR INFORMATION

Corresponding Author

*cheng-gong.sun@nottingham.ac.uk

ACKNOWLEDGEMENT

This work was supported by the UK Engineering and Physical Sciences Research Council [grant number EP/J020745/1]. We also thank Dr. Michael Fay for his kind assistance with transmission electron microscopy measurements and Nicola Weston for her kind assistance with scanning electron microscopy.

References

- (1) *World Energy Outlook Special Report 2015: Energy and Climate Change*. International Energy Agency (IEA), **2015**.
- (2) *Climate change 2014: synthesis Report*. Intergovernmental panel on climate change IPCC: Geneva, Switzerland, **2014**.
- (3) Mondal, M.; Balsora, H.; Varshney, P. Progress and trends in CO₂ capture/separation technologies: a review. *Energy* **2012**, *46*, 431-441.
- (4) Scott, V., Gilfillan, S., Markusson, N., Chalmers, H. and Haszeldine, R. Last chance for carbon capture and storage. *Nat. Clim. Change* **2012**, *3*, 105-111.

- (5) Shafeeyan, M. S.; Daud, W. M. A. W.; Houshmand, A.; Shamiri, A. A review on surface modification of activated carbon for carbon dioxide adsorption. *J. Anal. Appl. Pyrolysis* **2010**, *89*, 143-151.
- (6) D'Alessandro, D. M.; Smit, B.; Long, J. R. Carbon dioxide capture: prospects for new materials. *Angew. Chem. Int. Ed.* **2010**, *49*, 6058-6082.
- (7) Wang, J.; Huang, L.; Yang, R.; Zhang, Z.; Wu, J.; Gao, Y.; Wang, Q.; O'Hare, D.; Zhong, Z. Recent advances in solid sorbents for CO₂ capture and new development trends. *Energy. Environ. Sci.* **2014**, *7*, 3478-3518.
- (8) Wang, Q.; Luo, J.; Zhong, Z.; Borgna, A. CO₂ capture by solid adsorbents and their applications: current status and new trends. *Energy. Environ. Sci.* **2011**, *4*, 42-55.
- (9) Drage, T. C.; Snape, C. E.; Stevens, L. A.; Wood, J.; Wang, J.; Cooper, A. I.; Dawson, R.; Irons, R. Materials challenges for the development of solid sorbents for post-combustion carbon capture. *J. Mater. Chem.* **2012**, *22*, 2815-2823.
- (10) Dutcher, B.; Adidharma, H.; Radosz, M. Carbon filter process for flue-gas carbon capture on carbonaceous sorbents: steam-aided vacuum swing adsorption option. *Ind. Eng. Chem. Res.* **2011**, *50*, 9696-9703.
- (11) Plaza, M. G.; García, S.; Rubiera, F.; Pis, J. J.; Pevida, C. Post-combustion CO₂ capture with a commercial activated carbon: comparison of different regeneration strategies. *Chem. Eng. J.* **2010**, *163*, 41-47.
- (12) Plaza, M. G.; González, A. S.; Pis, J. J.; Rubiera, F.; Pevida, C. Production of microporous biochars by single-step oxidation: Effect of activation conditions on CO₂ capture. *Appl. Energy* **2014**, *114*, 551-562.
- (13) Morris, R. E.; Wheatley, P. S. Gas storage in nanoporous materials. *Angew. Chem. Int. Ed.* **2008**, *47*, 4966-4981.
- (14) Choi, S.; Drese, J. H.; Jones, C. W. Adsorbent materials for carbon dioxide capture from large anthropogenic point sources. *ChemSusChem* **2009**, *2*, 796-854.
- (15) Ma, X.; Li, Y.; Cao, M.; Hu, C. A novel activating strategy to achieve highly porous carbon monoliths for CO₂ capture. *J. Mater. Chem. A* **2014**, *2*, 4819-4826.

- (16) Liu, J.; Sun, N.; Sun, C.; Liu, H.; Snape, C.; Li, K.; Wei, W.; Sun, Y. Spherical potassium intercalated activated carbon beads for pulverised fuel CO₂ post-combustion capture *Carbon* **2015**, *94*, 243-255.
- (17) Himeno, S.; Komatsu, T.; Fujita, S. High-pressure adsorption equilibria of methane and carbon dioxide on several activated carbons. *J. Chem. Eng. Data* **2005**, *50*, 369-376.
- (18) Hao, G. P.; Li, W. C.; Qian, D.; Wang, G. H.; Zhang, W. P.; Zhang, T.; Wang, A.Q.; Schüth, F.; Bongard, H.J.; Lu, A. H. Structurally designed synthesis of mechanically stable poly (benzoxazine-co-resol)-based porous carbon monoliths and their application as high-performance CO₂ capture sorbents. *J. Am. Chem. Soc.* **2011**, *133*, 11378-11388.
- (19) Zhang, Z.; Zhou, J.; Xing, W.; Xue, Q.; Yan, Z.; Zhuo, S.; Qiao, S. Z. Critical role of small micropores in high CO₂ uptake. *Phys. Chem. Chem. Phys.* **2013**, *15*, 2523-2529.
- (20) Xu, C.; Bacsik, Z.; Hedin, N. Adsorption of CO₂ on a micro-/mesoporous polyimine modified with tris (2-aminoethyl) amine. *J. Mater. Chem. A* **2015**, *3*, 16229-16234.
- (21) Wan, L.; Wang, J.; Feng, C.; Sun, Y.; Li, K. Synthesis of polybenzoxazine based nitrogen-rich porous carbons for carbon dioxide capture. *Nanoscale* **2015**, *7*, 6534-6544.
- (22) Hao, G. P.; Li, W. C.; Qian, D.; Lu, A. H. Rapid Synthesis of Nitrogen-Doped Porous Carbon Monolith for CO₂ Capture. *Adv. Mater.* **2010**, *22*, 853-857.
- (23) Kim, Y. K.; Kim, G. M.; Lee, J. W. Highly porous N-doped carbons impregnated with sodium for efficient CO₂ capture. *J. Mater. Chem. A* **2015**, *3*, 10919-10927.
- (24) Sánchez-Sánchez, A.; Suárez-García, F.; Martínez-Alonso, A.; Tascón, J. M. Influence of porous texture and surface chemistry on the CO₂ adsorption capacity of porous carbons: acidic and basic site interactions. *ACS Appl. Mater. Interfaces* **2014**, *6*, 21237-21247.
- (25) Gadipelli, S.; Guo, Z. X. Tuning of ZIF-Derived Carbon with High Activity, Nitrogen Functionality, and Yield—A Case for Superior CO₂ Capture. *ChemSusChem* **2015**, *8*, 2123-2132.
- (26) Zhang, Z.; Xu, M.; Wang, H.; Li, Z. Enhancement of CO₂ adsorption on high surface area activated carbon modified by N₂, H₂ and ammonia. *Chem. Eng. J.* **2010**, *160*, 571-577.
- (27) Jang, D. I.; Park, S. J. Influence of nickel oxide on carbon dioxide adsorption behaviors of activated carbons. *Fuel* **2012**, *102*, 439-444.

- (28) Liu, L.; Deng, Q. F.; Ma, T. Y.; Lin, X. Z.; Hou, X. X.; Liu, Y. P.; Yuan, Z. Y. (2011). Ordered mesoporous carbons: citric acid-catalyzed synthesis, nitrogen doping and CO₂ capture. *J. Mater. Chem. A* **2011**, *21*, 16001-16009.
- (29) Wu, H.; Simmons, J. M.; Srinivas, G.; Zhou, W.; Yildirim, T. Adsorption sites and binding nature of CO₂ in prototypical metal-organic frameworks: A combined neutron diffraction and first-principles study. *J. Phys. Chem. Lett.* **2010**, *1*, 1946-1951.
- (30) Bae, T. H.; Hudson, M. R.; Mason, J. A.; Queen, W. L.; Dutton, J. J.; Sumida, K.; Micklash, K.J.; Kaye, S.S.; Brown, C.M.; Long, J. R. Evaluation of cation-exchanged zeolite adsorbents for post-combustion carbon dioxide capture. *Energy. Environ. Sci.* **2013**, *6*, 128-138.
- (31) Foo, K. Y.; Hameed, B. H. Mesoporous activated carbon from wood sawdust by K₂CO₃ activation using microwave heating. *Bioresour. Technol.* **2012**, *111*, 425-432.
- (32) Yahya, M. A.; Al-Qodah, Z.; Ngah, C. Z. Agricultural bio-waste materials as potential sustainable precursors used for activated carbon production: a review. *Renew. Sust. Energ. Rev.* **2015**, *46*, 218-235.
- (33) Kan, Y.; Yue, Q.; Kong, J.; Gao, B.; Li, Q. The application of activated carbon produced from waste printed circuit boards (PCBs) by H₃PO₄ and steam activation for the removal of malachite green. *Chem. Eng. J.* **2015**, *260*, 541-549.
- (34) Kalderis, D.; Bethanis, S.; Paraskeva, P.; Diamadopoulos, E. Production of activated carbon from bagasse and rice husk by a single-stage chemical activation method at low retention times. *Bioresour. Technol.* **2008**, *99*, 6809-6816.
- (35) Chen, Y.; Zhu, Y.; Wang, Z.; Li, Y.; Wang, L.; Ding, L.; Gao, X.; Ma, Y.; Guo, Y. Application studies of activated carbon derived from rice husks produced by chemical-thermal process-A review. *Adv. Colloid Interface Sci.* **2011**, *163*, 39-52.
- (36) Battezzore, D., Bocchini, S., Alongi, J., Frache, A. Rice husk as bio-source of silica: preparation and characterization of PLA-silica bio-composites. *RSC Adv.* **2014**, *4*, 54703-54712.
- (37) Gao, Y., Li, L., Jin, Y., Wang, Y., Yuan, C., Wei, Y.; Chen, G., Ge, J.; Lu, H. Porous carbon made from rice husk as electrode material for electrochemical double layer capacitor. *Appl. Energy* **2015**, *153*, 41-47.

- (38) Zhang, Y.; Song, X. L.; Huang, S. T.; Geng, B. Y.; Chang, C. H.; Sung, I. Y. Adsorption of nitrate ions onto activated carbon prepared from rice husk by NaOH activation. *Desalination Water Treat.* **2014**, *52*, 4935-4941.
- (39) Yeletsky, P. M., Yakovlev, V. A., Mel'gunov, M. S., Parmon, V. N. Synthesis of mesoporous carbons by leaching out natural silica templates of rice husk. *Micropor. Mesopor. Mat.* **2009**, *121*, 34-40.
- (40) Cheenmatchaya, A., Kungwankunakorn, S. Preparation of activated carbon derived from rice husk by simple carbonization and chemical activation for using as gasoline adsorbent. *Int. J. Environ. Sci. Technol.* **2014**, *5*, 171-175.
- (41) Lee, S. Y.; Park, S. J. Carbon dioxide adsorption performance of ultramicroporous carbon derived from poly (vinylidene fluoride). *J Anal. Appl. Pyrolysis* **2014**, *106*, 147-151.
- (42) Li, J.; Lu, R.; Dou, B.; Ma, C.; Hu, Q.; Liang, Y.; Wu, F.; Qiao, S.; Hao, Z. Porous graphitized carbon for adsorptive removal of benzene and the electrothermal regeneration. *Environ. Sci. Technol.* **2012**, *46*, 12648-12654.
- (43) Wang, M.; Wang, J.; Qiao, W.; Ling, L.; Long, D. Scalable preparation of nitrogen-enriched carbon microspheres for efficient CO₂ capture. *RSC Adv.* **2014**, *4*, 61456-61464.
- (44) Wang, H.; Gao, Q.; Hu, J. High hydrogen storage capacity of porous carbons prepared by using activated carbon. *J. Am. Chem. Soc.* **2009**, *131*, 7016-7022.
- (45) Kim, B. J.; Lee, Y. S.; Park, S. J. A study on pore-opening behaviors of graphite nanofibers by a chemical activation process. *J. Colloid Interface Sci.* **2007**, *306*, 454-458.
- (46) Meng, L. Y.; Meng, W.; Chen, T.; Jin, L. Y. CO₂ Adsorption capacity of activated N-doping porous carbons prepared from graphite nanofibers/polypyrrole. *J. Appl. Polym. Sci.* **2014**, *131*, 40517.
- (47) Yang, S., Hu, H., & Chen, G. Preparation of carbon adsorbents with high surface area and a model for calculating surface area. *Carbon* **2002**, *40*, 277-284.
- (48) Nandi, S.; De Luna, P.; Daff, T. D.; Rother, J.; Liu, M.; Buchanan, W.; Hawari, A.I.; Woo, T.K.; Vaidhyanathan, R. A single-ligand ultra-microporous MOF for precombustion CO₂ capture and hydrogen purification. *Sci. Adv.* **2015**, *1*, e1500421.

- (49) Sethia, G.; Sayari, A. Comprehensive study of ultra-microporous nitrogen-doped activated carbon for CO₂ capture. *Carbon* **2015**, *93*, 68-80.
- (50) Yahya, M. A.; Al-Qodah, Z.; Ngah, C. Z. Agricultural bio-waste materials as potential sustainable precursors used for activated carbon production: a review. *Renew. Sust. Energ. Rev.* **2015**, *46*, 218-235.
- (51) Lanning, F. C. (1963). Plant constituents, silicon in rice. Plant constituents, silicon in rice. *J. Agric. Food Chem.* **1963**, *11*, 435-437.
- (52) Freitas, J. C.; Schettino, M. A.; Cunha, A. G.; Emmerich, F. G.; Bloise, A. C.; De Azevedo, E. R.; Bonagamba, T. J. NMR investigation on the occurrence of Na species in porous carbons prepared by NaOH activation. *Carbon* **2007**, *45*, 1097-1104.
- (53) Otowa, T.; Tanibata, R.; Itoh, M. Production and adsorption characteristics of MAXSORB: high-surface-area active carbon. *Gas Sep. Purif.* **1993**, *7*, 241-245.
- (54) Jiménez, V.; Ramírez-Lucas, A.; Díaz, J. A.; Sánchez, P.; Romero, A. CO₂ capture in different carbon materials. *Environ Sci Technol.* **2012**, *46*, 7407-7414.
- (55) Marsh, H.; Yan, D. S.; O'Grady, T. M.; Wennerberg, A. Formation of active carbons from cokes using potassium hydroxide. *Carbon* **1984**, *22*, 603-611.
- (56) Shen, Z.; Xue, R. Preparation of activated mesocarbon microbeads with high mesopore content. *Fuel processing technol.* **2003**, *84*, 95-103.
- (57) Addoun, A.; Dentzer, J.; Ehrburger, P. Porosity of carbons obtained by chemical activation: effect of the nature of the alkaline carbonates. *Carbon* **2002**, *40*, 1140-1143.
- (58) McKee, D. W. (1983). Mechanisms of the alkali metal catalysed gasification of carbon. *Fuel* **1983**, *62*, 170-175.
- (59) Yeletsky, P. M.; Yakovlev, V. A.; Mel'gunov, M. S.; Parmon, V. N. Synthesis of mesoporous carbons by leaching out natural silica templates of rice husk. *Micropor. Mesopor. Mat.* **2009**, *121*, 34-40.
- (60) Wang, W.; Martin, J. C.; Fan, X.; Han, A.; Luo, Z.; Sun, L. Silica nanoparticles and frameworks from rice husk biomass. *ACS Appl. Mater. Interfaces* **2012**, *4*, 977-981.
- (61) Presser, V.; McDonough, J.; Yeon, S. H.; Gogotsi, Y. Effect of pore size on carbon dioxide sorption by carbide derived carbon. *Energy. Environ. Sci.* **2011**, *4*, 3059-3066.

- (62) Wickramaratne, N. P.; Jaroniec, M. Importance of small micropores in CO₂ capture by phenolic resin-based activated carbon spheres. *J. Mater. Chem. A* **2013**, *1*, 112-116.
- (63) Zhao, Y.; Liu, X.; Yao, K. X.; Zhao, L.; Han, Y. Superior capture of CO₂ achieved by introducing extra-framework cations into N-doped microporous carbon. *Chem. Mater.* **2012**, *24*, 4725-4734.
- (64) Pirngruber, G. D.; Raybaud, P.; Belmabkhout, Y.; Čejka, J.; Zukul, A. The role of the extra-framework cations in the adsorption of CO₂ on faujasite Y. *Phys. Chem. Chem. Phys.* **2010**, *12*, 13534-13546.
- (65) Pulido, A.; Nachtigall, P.; Zukul, A.; Domínguez, I.; Čejka, J. Adsorption of CO₂ on sodium-exchanged ferrierites: the bridged CO₂ complexes formed between two extra framework cations. *J. Phys. Chem. C* **2009**, *113*, 2928.
- (66) RAAB, C. G. D. I. R. Measurement of the electric quadrupole moments of CO₂, CO, N₂, Cl₂ and BF₃. *Mol. Phys.* **1998**, *93*, 49-56.
- (67) Martin-Calvo, A.; Parra, J. B.; Ania, C. O.; Calero, S. Insights on the anomalous adsorption of carbon dioxide in LTA zeolites. *J. Phys. Chem. C* **2014**, *118*, 25460-25467.
- (68) Li, S.; Kang, E. T.; Neoh, K. G.; Ma, Z. H.; Tan, K. L.; Huang, W. In situ XPS studies of thermally deposited potassium on poly (p-phenylene vinylene) and its ring-substituted derivatives. *Appl. Surf. Sci.* **2001**, *181*, 201-210.
- (69) Moulder, J. F.; Stickle, W.F.; Bomben, K.D. In: J. Chastain (Ed.), *Handbook of X-ray Photoelectron Spectroscopy*, Perkin Elmer, Eden Prairie, MN, **1992**, 66-67.
- (70) Shchukarev, A.; Korolkov, D. XPS Study of group IA carbonates. *Open Chem.* **2004**, *2*, 347-362.
- (71) Barr, T. L. An XPS study of Si as it occurs in adsorbents, catalysts, and thin films. *Appl. Surf. Sci.* **1983**, *15*, 1-35.
- (72) Miller, M. L.; Linton, R. W. X-ray photoelectron spectroscopy of thermally treated silica (SiO₂) surfaces. *Anal. Chem.* **1985**, *57*, 2314-2319.
- (73) Stipp, S. L.; Hochella, M. F. Structure and bonding environments at the calcite surface as observed with X-ray photoelectron spectroscopy (XPS) and low energy electron diffraction (LEED). *Geochim. Cosmochim. Acta.* **1991**, *55*, 1723-1736.
- (74) Zhang, W.; Li, X.; Qu, Z.; Zhao, Q.; Chen, G. Facile solution synthesis and characterization of CaCO₃ microspheres with urchin-shaped structure. *Mater. Lett.* **2010**, *64*, 71-73.

- (75) Zhang, W., Liu, H., Sun, Y., Cakstins, J., Sun, C., Snape, C. E. Parametric study on the regeneration heat requirement of an amine-based solid adsorbent process for post-combustion carbon capture. *Appl. Energ.* **2016**, *168*, 394-405.
- (76) Rege, S. U.; Yang, R. T.; Buzanowski, M. A. Sorbents for air prepurification in air separation. *Chem. Eng. Sci.* **2000**, *55*, 4827-4838.
- (77) Farrusseng, D.; Daniel, C.; Gaudillere, C.; Ravon, U.; Schuurman, Y.; Mirodatos, C.; Dubbeldam, D.; Frost, H.; Snurr, R. Q. Heats of adsorption for seven gases in three metal- organic frameworks: systematic comparison of experiment and simulation. *Langmuir* **2009**, *25*, 7383-7388.
- (78) Li, J. R.; Ma, Y.; McCarthy, M. C.; Sculley, J.; Yu, J.; Jeong, H. K.; Balbuena, P.B.; Zhou, H. C. Carbon dioxide capture-related gas adsorption and separation in metal-organic frameworks. *Coord. Chem. Rev.* **2011**, *255*, 1791-1823.

Table of Contents

